

Original paper

# Molecular structure of the phosphate mineral koninckite – – a vibrational spectroscopic study

Jakub JIRÁSEK<sup>1\*</sup>, Jiří ČEJKA<sup>2</sup>, Luboš VRTIŠKA<sup>2,3</sup>, Dalibor MATÝSEK<sup>1</sup>, Xiuxiu RUAN<sup>4</sup>,  
Ray L. FROST<sup>4</sup>

<sup>1</sup> Institute of Geological Engineering, Faculty of Mining and Geology, VŠB – Technical University of Ostrava, 17. listopadu 15/2172, 708 33 Ostrava-Poruba, Czech Republic; jakub.jirasek@vsb.cz

<sup>2</sup> Department of Mineralogy and Petrology, National Museum, Cirkusová 1740, 193 00 Prague – Horní Počernice, Czech Republic

<sup>3</sup> Department of Geological Sciences, Faculty of Science, Masaryk University, Kotlářská 2, 611 37 Brno, Czech Republic

<sup>4</sup> School of Chemistry, Physics and Mechanical Engineering, Science and Engineering Faculty, Queensland University of Technology, GPO Box 2434, Brisbane Queensland 4001, Australia

\* Corresponding author



We have undertaken a study of the mineral koninckite from Litošice (Czech Republic), a hydrated ferric phosphate, using a combination of scanning electron microscopy with electron probe micro-analyzer (wavelength-dispersive spectroscopy) and vibrational spectroscopy. Chemical analysis shows that studied koninckite is a pure phase with an empirical formula  $\text{Fe}^{3+}_{0.99}(\text{PO}_4)_{1.00} \cdot 2.75 \text{H}_2\text{O}$ , with minor enrichment in Al, Ca, Ti, Si, Zn, and K (averages 0.00X *apfu*). Raman bands and shoulders at 3495, 3312, 3120, and 2966  $\text{cm}^{-1}$  and infrared bands and shoulders at 3729, 3493, 3356, 3250, 3088, 2907, and 2706  $\text{cm}^{-1}$  are assigned to the  $\nu$  OH stretching of structurally distinct differently hydrogen bonded water molecules. A Raman band at 1602  $\text{cm}^{-1}$  and shoulders at 1679, 1659, 1634, and 1617  $\text{cm}^{-1}$  and infrared bands at 1650 and 1598  $\text{cm}^{-1}$  are assigned to the  $\nu_2$  ( $\delta$ )  $\text{H}_2\text{O}$  bending vibrations of structurally distinct differently hydrogen bonded water molecules. Raman shoulders at 1576, 1554, 1541, 1532, and 1520  $\text{cm}^{-1}$  and infrared shoulders at 1541 and 1454  $\text{cm}^{-1}$  may be probably connected with zeolitically bonded water molecules located in the channels. Raman bands and shoulders at 1148, 1132, 1108, 1063, 1048, and 1015  $\text{cm}^{-1}$  and an infrared band and shoulders at 1131, 1097, 1049, and 1017  $\text{cm}^{-1}$  are assigned to the  $\nu_3$   $\text{PO}_4^{3-}$  triply degenerate antisymmetric stretching vibrations. A Raman band and a shoulder at 994 and 970  $\text{cm}^{-1}$ , respectively, and an infrared band and a shoulder at 978 and 949  $\text{cm}^{-1}$ , respectively, are assigned to the  $\nu_1$   $\text{PO}_4^{3-}$  symmetric stretching vibrations. Infrared shoulders at 873, 833, and 748  $\text{cm}^{-1}$  are assigned to libration modes of water molecules. Raman bands and shoulders at 670, 648, 631, 614, 600, 572, and 546  $\text{cm}^{-1}$  and infrared bands at 592 and 534  $\text{cm}^{-1}$  are assigned to the  $\nu_4$  ( $\delta$ )  $\text{PO}_4^{3-}$  triply degenerate out-of-plane bending vibrations; weak band at 570  $\text{cm}^{-1}$  may coincide with the  $\delta$  Fe–O bending vibration. Raman bands and shoulders at 453, 443, 419, and 400  $\text{cm}^{-1}$  are assigned to the  $\nu_2$  ( $\delta$ )  $\text{PO}_4^{3-}$  doubly degenerate in-plane bending vibrations. Raman bands at 385, 346, 324, 309, 275, 252, and 227  $\text{cm}^{-1}$  are assigned to the  $\nu$  Fe–O stretching vibrations in  $\text{FeO}_6$  octahedra. Raman bands at 188, 158, 140, 112, 89, and 73  $\text{cm}^{-1}$  are assigned to lattice vibrations.

**Keywords:** koninckite, phosphate, Raman spectroscopy, infrared spectroscopy

**Received:** 3 October 2016; **accepted:** 6 October 2017; **handling editor:** J. Sejkora

## 1. Introduction

Koninckite is a natural phosphate mineral of formula  $\text{Fe}^{3+}(\text{PO}_4) \cdot 2.75\text{H}_2\text{O}$ . It was named by Cesàro (1884) after Professor Laurent Guillaume de Koninck (1809–1887), notable Belgian paleontologist and chemist. Type locality is Richelle near Visé (Belgium). The mineral forms yellowish, white and colorless coatings, veins and rarely also crystal aggregates.

Koninckite belongs to the tetragonal crystal system. Published cell parameters are given in Tab. 1. The crystal structure of koninckite was solved recently by Plášil et al. (2015) from synchrotron powder X-ray diffraction data. Investigated material from Kociha (Slovakia) is tetragonal, with the space group  $P4_12_12$ . Its crystal structure is

built as a heteropolyhedral framework with zeolite-like tunnels along [001]. The  $\text{Fe}^{3+}$  ions in the structure are in octahedral coordination by  $\text{H}_2\text{O}$  molecules and oxygen ions of the  $\text{PO}_4^{3-}$  tetrahedra. Koninckite should be an antiferromagnetic semiconductor, at least at low temperatures.

Summary of all known occurrences of koninckite and associated secondary minerals was given in Jirásek (2005) and Plášil et al. (2015). Circa 20 localities are known worldwide. Most often koninckite is associated with hydrated sulphates of Fe, Al and Mn in places of acid weathering of various phosphorous-rich rocks at shallow depths. At Richelle, Belgium (Van Tassel 1968), Nekézseny and Dédestapolcsány, Hungary (Koch 1985; Szakáll and Gatter 1993; Szakáll ed.

**Tab. 1** Lattice cell parameters of koninckite

Locality	Source	<i>a</i> (Å)	<i>c</i> (Å)
Litošice (Czech Republic)	this study	11.9762(2)	14.6209(3)
Kociha (Slovakia)	Plášil et al. (2015)	11.9800(5)	14.618(1)
Kociha (Slovakia)	Novák et al. (2003)	11.956(6)	14.543(8)
Suwa Mine (Japan)	Sakurai et al. (1987)	11.977(2)	14.625(2)
Richelle (Belgium)	Van Tassel (1968)	11.95(5)	14.52(8)

2002), Arnsberg (Blaß and Graf 1990) and Hardtkopf (Blaß and Graf 1995), both in Germany, and Shanagolden, Republic of Ireland (Moreton and Green 2005), it originates by weathering of Carboniferous sedimentary rocks. At Oberbuchach, Austria (Leute 1996; Von Puttner 1997) and Montcada, Spain (Riba 1997) the source sediments are clayey Silurian shales. Cambro–Ordovician black shales are source rocks at Kociha, Slovakia (Novák et al. 2003), and Upper Proterozoic black shales in Litošice, Czech Republic (Jirásek 2005). At Untersulzbachtal, Austria (Burgsteiner 1997 in Leute 1999) source rocks are kyanite schists. Kovdor Massif, Russia yielded koninckite from apatite-rich fenite (Ivanyuk and Yakovenchuk 1987). Zoned concretions with koninckite from the Ponta Grosse Fm., Paraná Basin, Brazil, originate by lateritic weathering of Devonian sediments (Leonardos et al. 1987). Supergene koninckite was found in apatite-rich barren rock at base metal deposit of Pollone, Italy (Senesi 2000).

Exceptional origin of koninckite was described at four localities. At Kyrk-Bulak, Kyrgyzstan, Mn-rich koninckite is produced by decomposition of heterosite and strengite in granitic pegmatites (Beus 1950, 1951). At Oni-Ana, Japan, is koninckite present in cave sediments (Kizaki 1983 in Sakurai et al. 1987). At Suwa Mine, Japan, this mineral originates by interaction of hot hydrothermal solutions rich in Fe<sup>3+</sup> and SO<sub>4</sub><sup>2-</sup> with andesites and volcanoclastic rocks (Sakurai et al. 1987). Similar processes might be suspected for koninckite formation at New Idria Mine, California, USA, although there is only a short notice available about presence of the investigated mineral (Symons 1937).

Even though the work on the koninckite crystal structure has been published recently, Raman and infrared spectroscopic studies have not been conducted so far. Still, Raman spectroscopy has proven an excellent technique for the study of oxyanions in both solution and in secondary mineral formation (e.g., Frost et al. 2013a, b; 2014). The aim of this paper is therefore to report the Raman spectra of koninckite, and to relate the spectra to the molecular structure of this phosphate mineral. The paper follows the systematic research of the large group of supergene minerals and especially molecular structure of minerals containing oxyanions using infrared (IR) and Raman spectroscopy.

## 2. Material and methods

### 2.1. Samples description and preparation

The koninckite sample studied in this work comes from the Litošice, Pardubice Region, Czech Republic (N 49° 58.935' E 015° 29.968'). It was described by Jirásek (2005). Material was found in a small dump of abandoned iron and manganese prospect, which explored southern end of belt of Neoproterozoic marine black pyritic shales. These shales were interpreted as a product of submarine volcanic activity and were exploited in 19<sup>th</sup> and 20<sup>th</sup> centuries as a Fe–Mn ore and source of pyrite for chemical industry. Koninckite is present as white to beige veinlets up to 1 cm thick in the porous brownish amorphous phosphate historically described as delvauxite (possible diadochite). Macroscopically it looks massive, but small prismatic crystals up to *c.* 10 µm are visible in microscopic cavities by electron microscope.

The koninckite sample studied in this work occurs in association with dolomite. It was gently crushed and the associated minerals were removed under a Leica MZ4 stereomicroscope. Scanning electron microscopy (SEM) in the EDS mode was applied to support the mineral characterization.

### 2.2. Electron microscopy and microanalysis

The surface morphology of the samples was studied using scanning electron microscopy (FEI Quanta 650 FEG microscope equipped with energy-dispersive, wavelength-dispersive, electron backscatter diffraction and cathodoluminescence detectors) at Faculty of Mining and Geology, VŠB – Technical University of Ostrava. Microphotographs of separated, untreated and unpolished grains fixed on a graphite holder without coating were made by back-scattered electron (BSE) detector.

The chemical composition of koninckite was determined using an electron microprobe Cameca SX 100 (Joint Laboratory of the Masaryk University and Czech Geological Survey, Brno). Wavelength dispersive mode and following conditions were used: accelerating voltage of 15 keV, beam current of 10 nA and beam diameter of 10 µm; analytical lines K<sub>α</sub>; standards: Na (albite), Si, Al, K (sanidine), Mg (pyrope), P (fluorapatite), Ti (titanite),

Ca (wollastonite), Fe (almandine), Mn (spessartine), Zn (gahnite), F (topaz). The raw data were processed using the X- $\phi$  matrix correction routine (Merlet 1994).

### 2.3. Powder X-ray diffraction

X-ray powder diffraction (XRD) measurements were conducted using a Bruker-AXS D8 Advance instrument (at VŠB – Technical University of Ostrava) with the 2 $\theta$ / $\theta$  geometry using a silicon strip LynxEye position-sensitive detector under the following conditions: radiation CoK $\alpha$ /Fe filter, voltage 40 kV, current 40 mA, step by step mode of 0.014 2 $\theta$ . The samples were placed on a zero-background rotating single-crystal Si slide and scanned. A total time on step 46.25 s and angular extent 5–140° 2 $\theta$  were used. 5.6 wt. % of Si (NIST 640c) was added as internal standard for the measurement.

The data were digitally processed using the Bruker AXS Diffrac and Bruker EVA software and the PDF-2 database (2011 release; International Centre for Diffraction Data). The cell parameters and quantitative composition of the investigated sample were determined by the Rietveld method (Bruker Topas 4.2 software). Structural information published by Plášil et al. (2015) was used.

### 2.4. Raman and infrared spectroscopy

Raman spectra of the studied sample were collected at room temperature in the range 50–4000 cm $^{-1}$  using a DXR dispersive Raman Spectrometer (Thermo Scientific) mounted on confocal Olympus microscope (National Museum, Prague). The Raman signal was excited by an unpolarized 532 nm diode-pumped solid-state laser and detected by a CCD detector. The experimental parameters were: 20 $\times$  objective (estimated diameter of the laser spot less than 1.3  $\mu$ m), 6 s exposure time, 3600 exposures, 830 lines/mm grating (spectral resolution better than 3 cm $^{-1}$ ), 50  $\mu$ m pinhole spectrograph aperture and 6 mW laser power level. The data were repeatedly acquired from different grains in order to obtain a representative spectrum with the best signal to noise ratio. Eventual thermal damage of the measured point was excluded by visual inspection of excited surface after measurement, by observation of possible decay of spectral features in the start of excitation and checking for thermal downshift of Raman lines.

The instrument was set up by a software-controlled calibration procedure using multiple neon emission lines (wavelength calibration), multiple polystyrene Raman bands (laser frequency calibration) and standardized white-light sources (intensity calibration).

The infrared vibrational spectrum of koninckite was recorded by the attenuated total reflection (ATR) method with the diamond cell on a Nicolet iS5 spectrometer at the

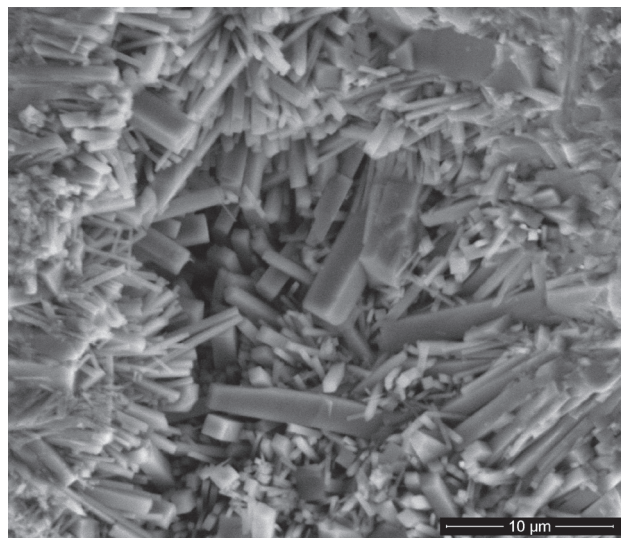


**Fig. 1** Backscattered electron image of an aggregate of columnar koninckite crystals.

National Museum, Prague. Spectra over the 4000–525 cm $^{-1}$  range were obtained by the co-addition of 128 scans with a resolution of 4 cm $^{-1}$  and a mirror velocity of 0.4747 cm/s. Spectra were co-added to improve the signal to noise ratio.

Spectral manipulations were performed using the Omnic 9 software (Thermo Scientific). Gaussian/Lorentzian profile functions of the band-shape were used to obtain decomposed band components of the spectra. The decomposition was based on the minimization of the difference in the observed and calculated profiles until the squared correlation coefficient ( $r^2$ ) was greater than 0.995.

## 3. Results and discussion

### 3.1. Chemical characterization

The BSE image of koninckite sample studied in this work is shown in Fig. 1. The sample corresponds to an aggregate of crystals up to 20  $\mu$ m long. New WDS data confirm previously published EDS analysis (Jirásek 2005) and reveal chemically almost pure koninckite. The empirical formula of koninckite, calculated as the mean of 7 representative spot analyses (Tab. 2), is Fe $^{3+}_{0.99}$ (PO $_4$ ) $_{1.00}$ ·2.75 H $_2$ O (based on 4 O and 2.75 H $_2$ O *apfu*). It shows minor Al (average 0.005 *apfu*), Ca (average 0.004 *apfu*), Ti (average 0.003 *apfu*) and K (average 0.002 *apfu*). Some analyses also contained up to 0.003 *apfu* of Zn, 0.003 *apfu* of Na, 0.002 *apfu* of Mg, and 0.009 *apfu* of F.

### 3.2. X-ray diffraction

Positions of the diffraction lines of the studied sample (Fig. 2) are in good agreement with the published ones

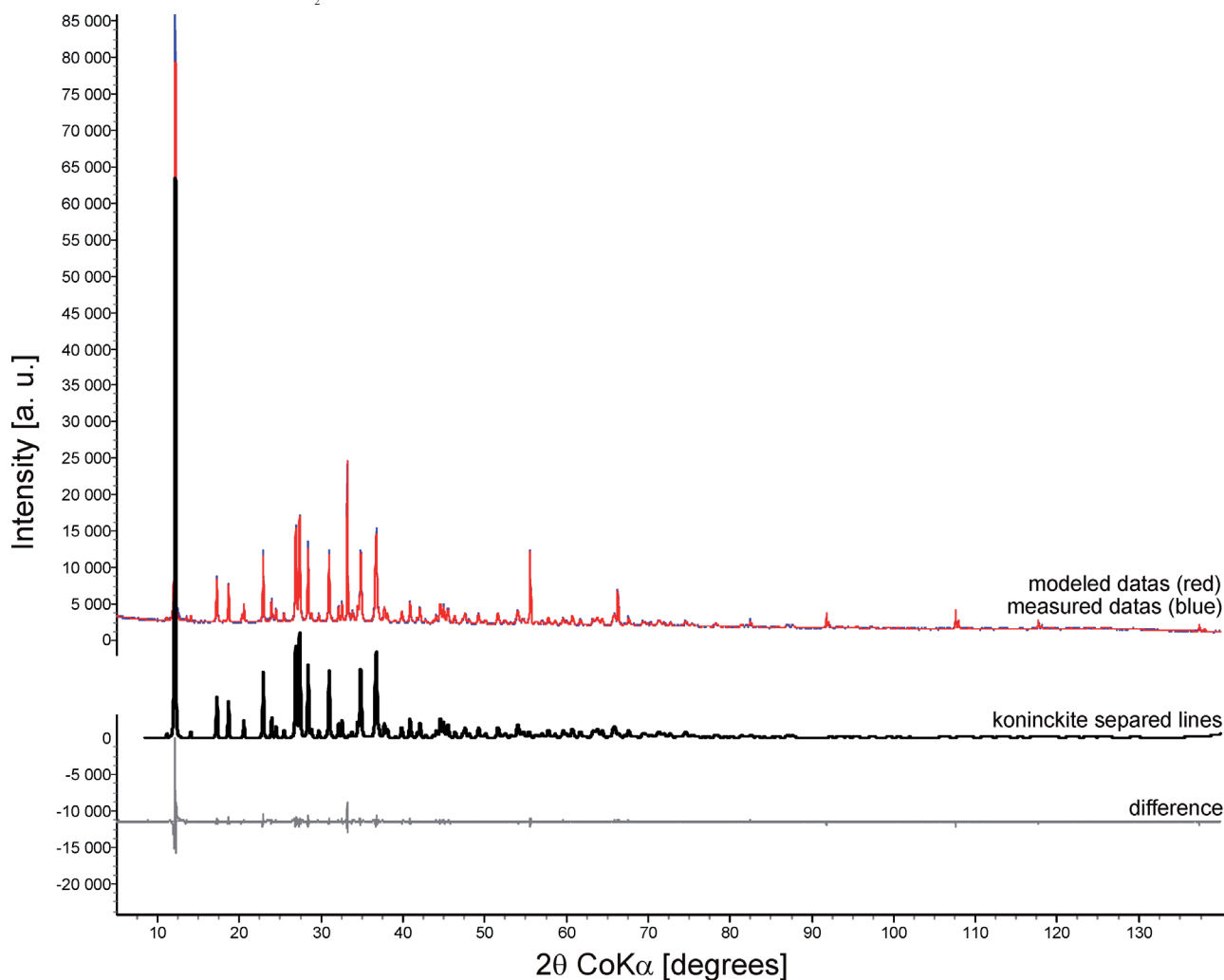
**Tab. 2** Chemical composition of the studied koninckite (wt. % and *apfu*)

	1	2	3	4	5	6	7
P <sub>2</sub> O <sub>5</sub>	34.25	34.37	34.03	34.15	35.25	33.76	34.01
Al <sub>2</sub> O <sub>3</sub>	0.09	0.11	0.18	0.11	0.09	0.10	0.14
Fe <sub>2</sub> O <sub>3</sub>	37.93	38.14	37.90	38.23	39.28	38.15	37.96
SiO <sub>2</sub>	–	0.04	–	0.04	–	–	0.08
TiO <sub>2</sub>	0.14	0.13	0.13	0.09	0.08	0.09	0.11
CaO	0.06	0.16	0.07	0.07	0.08	0.16	0.09
ZnO	–	0.10	0.09	0.13	–	0.07	0.01
K <sub>2</sub> O	0.04	0.04	–	0.04	0.04	0.04	0.04
H <sub>2</sub> O*	23.51	23.65	23.49	23.70	24.35	23.65	23.53
Total	96.02	96.74	95.89	96.56	99.17	96.02	95.97
P <sup>5+</sup>	1.001	0.997	0.997	0.995	0.997	0.991	0.995
Al <sup>3+</sup>	0.004	0.005	0.007	0.005	0.003	0.004	0.006
Fe <sup>3+</sup>	0.986	0.984	0.987	0.990	0.988	0.996	0.987
Si <sup>4+</sup>	–	0.001	–	0.001	–	–	0.003
Ti <sup>4+</sup>	0.004	0.003	0.003	0.002	0.002	0.002	0.003
Ca <sup>2+</sup>	0.002	0.006	0.002	0.003	0.003	0.006	0.003
Zn <sup>2+</sup>	–	0.003	0.002	0.003	–	0.002	–
K <sup>+</sup>	0.002	0.002	–	0.002	0.002	0.002	0.002
H <sub>2</sub> O**	2.750	2.750	2.750	2.750	2.750	2.750	2.750

 \* calculated on the basis of Fe<sup>3+</sup>/H<sub>2</sub>O ratio

 \*\* calculated on the basis of 2.75 H<sub>2</sub>O in ideal formula of koninckite

(PDF 00-041-1489). Diffraction pattern of koninckite is given in Tab. 3. Material shows minor (< 1.5 %) admixture of gypsum and jarosite. Due to the internal standard utilization it is clear that the investigated sample contains significant amount of the amorphous matter (*c.* 32 %). Published structural data (Plášil et al. 2015) are in a good agreement with the observed ones ( $R_{wp} = 7.0\%$ ,  $R_{exp} = 1.99\%$ ,  $GOF = 3.5\%$ ). Small differences in intensities can be ascribed to the partial dehydration, since water is not stable bonded in the structure. The refined unit-cell parameters  $a = 11.9762(2)$  Å and  $c = 14.6209(3)$  Å are very similar to the published data (Tab. 1).


**Fig. 2** Powder XRD pattern of koninckite.

**Tab. 3** Powder X-ray diffraction data of studied koninckite

$d_{\text{obs}}$ (Å)	$I_{\text{rel}}$ (%)	$d_{\text{calc}}$ (Å)	$F^2$	h k l
8.4364	100	8.46872	60.51	1 1 0
5.9712	8	5.98829	10.33	0 2 0
5.5190	7	5.53394	6.76	1 1 2
5.0169	3	5.02927	6.56	2 1 1
4.5040	12	4.51432	22.96	0 1 3
4.3117	4	4.32061	11.31	2 1 2
4.2157	2	4.22421	3.50	1 1 3
3.8433	16	3.85122	75.27	0 3 1
3.7798	18	3.78733	78.71	3 1 0
3.6490	13	3.65535	36.80	0 0 4
3.3511	12	3.35607	42.72	1 1 4
3.2344	3	3.23917	14.61	3 2 1
3.1914	3	3.19648	17.71	2 2 3
3.0191	3	3.01924	1.03	2 1 4
2.9886	12	2.99414	100.46	0 4 0
2.8379	16	2.84083	59.99	0 1 5
2.7670	2	2.77077	17.86	0 4 2
2.5635	4	2.56665	35.14	2 1 5
2.4917	3	2.49520	22.78	4 1 3
2.3610	3	2.36381	41.27	4 3 1
2.3396	3	2.34187	26.03	1 1 6
2.3192	3	2.31907	14.72	5 1 1
2.2168	2	2.21811	13.50	2 1 6
1.9703	2	1.97224	34.45	0 2 7
1.9190	12	1.92561	26.45	0 6 2
1.9150	6	1.90119	9.87	6 1 2
1.6451	2	1.64603	34.26	3 1 8
1.6367	6	1.63323	10.68	6 1 5
1.1084	2	1.10752	26.77	7 5 8

Only values for  $I_{\text{rel}} \geq 2\%$  are given for simplicity

### 3.3. Raman and infrared spectroscopy

In the crystal structure of tetragonal mineral koninckite,  $\text{FePO}_4 \cdot 2.75 \text{H}_2\text{O}$ , space group  $P4_12_1 - D_{4d}^4$ ,  $Z = 16$ , are

**Tab. 4** Tentative interpretation of Raman and infrared spectra of koninckite

Raman ( $\text{cm}^{-1}$ )	Infrared ( $\text{cm}^{-1}$ )	Assignment
3495(sh), 3312(m), 3120(m), 2966(sh)	3729(sh), 3493(sh), 3356(sh), 3250(m), 3088(w), 2907(sh), 2706(sh)	$\nu$ OH stretching vibrations of structurally distinct differently hydrogen bonded water molecules
1679(sh), 1659(sh), 1634(sh), 1617(sh)	1650(sh), 1598(m)	$\nu_2$ ( $\delta$ ) $\text{H}_2\text{O}$ bending vibrations of structurally distinct differently hydrogen bonded water molecules
1576(sh), 1554(sh), 1541(sh), 1532(sh), 1520(sh)	1541(vw), 1454(vw)	$\nu_2$ ( $\delta$ ) $\text{H}_2\text{O}$ bending vibrations of zeolitically bonded water molecules located in the channels
1148(vw), 1132(w), 1108(vw), 1063(m), 1048(m), 1015(m)	1131(m), 1097(sh), 1049(sh), 1017(sh)	$\nu_3$ $\text{PO}_4^{3-}$ triply degenerate antisymmetric stretching vibrations
994(vs), 970(sh)	978(ms), 949(sh) 873(sh), 833(sh), 748(sh)	$\nu_1$ $\text{PO}_4^{3-}$ symmetric stretching vibrations vibration modes of water molecules
670(vw), 648(vw), 631(vw), 614(vw), 600(w), 572(m), 546(vw)	592(w), 534(vw)	$\nu_4$ ( $\delta$ ) $\text{PO}_4^{3-}$ triply degenerate out-of-plane bending vibrations; weak band at $570 \text{ cm}^{-1}$ may coincide with the $\delta$ Fe–O bending vibration
453(sh), 443(m), 419(sh), 400(sh)		$\nu_2$ ( $\delta$ ) $\text{PO}_4^{3-}$ doubly degenerate in-plane bending vibrations
385(w), 346(m), 324(m), 309(w), 275(w), 252(m), 227(m)		$\nu$ Fe–O stretching vibrations in $\text{FeO}_6$ octahedra
188(w), 158(w), 140(w), 112(m), 89(w), 73(m)		lattice vibrations

Abbreviations: sh – shoulder, m – medium, w – weak, vw – very weak.

present structurally distinct 2  $\text{Fe}^{3+}$  and 2  $\text{P}^{5+}$  units (Plášil et al. 2015). In the case of a free  $\text{PO}_4^{3-}$  ion of  $T_d$  symmetry, there are nine normal vibrations characterized by four fundamental distinguishable modes of vibration:  $\nu_1$  ( $A_1$ ) symmetric stretching vibration, Raman active ( $\sim 938 \text{ cm}^{-1}$ );  $\nu_2$  ( $E$ ) doubly degenerate in-plane bending vibration, Raman active ( $\sim 420 \text{ cm}^{-1}$ );  $\nu_3$  ( $F_2$ ) triply degenerate antisymmetric stretching vibration, Raman and infrared active ( $\sim 1017 \text{ cm}^{-1}$ );  $\nu_4$  ( $F_2$ ) triply degenerate out-of-plane bending vibration, Raman and infrared active ( $\sim 527 \text{ cm}^{-1}$ ) (Nakamoto 2009). In the case of symmetry lowering e.g.  $T_d \rightarrow C_{3v}, C_{2v}, C_1$ , the  $\nu_1$   $\text{PO}_4^{3-}$  symmetric stretching vibration is activated and can appear in the IR spectrum. A decrease of symmetry is also the cause of IR activation and splitting of the  $\nu_2$   $\text{PO}_4^{3-}$  doubly degenerate bending vibration. Simultaneously, the  $\nu_3$   $\text{PO}_4^{3-}$  triply degenerate antisymmetric stretching vibration and the  $\nu_4$   $\text{PO}_4^{3-}$  bending vibration, both active in the IR and Raman spectra, can split into two or three components (Nakamoto 2009). Chukanov (2014) included in his atlas of spectra of minerals infrared spectrum of koninckite ( $\text{cm}^{-1}$ ): 3480 sh, 3260, 3145, 1640, 1140s, 1052 s, 1025 sh, 996 s, 875 w, 846 w, 770 w., 606, 540. This spectrum differs from the IR spectrum of koninckite presented in this paper. Raman and infrared spectra of the studied mineral koninckite are given in Fig. 3, tabularized values in Tab. 4.

Raman weak broad bands at 3312 and 3120  $\text{cm}^{-1}$  with shoulders at 3495 and 2966  $\text{cm}^{-1}$  (Fig. 4a) and infrared broad bands at 3250 and 3088  $\text{cm}^{-1}$  with shoulders at 3729, 3493, 3356, 2907 and 2706  $\text{cm}^{-1}$  (Fig. 5a) are assigned to the  $\nu$  OH stretching vibrations of structurally distinct and differently strong hydrogen bonded water molecules. According to Libowitzky's empirical relation (Libowitzky 1999), O–H $\cdots$ O hydrogen bond lengths vary approximately in the ranges  $>3.2$ – $2.65 \text{ \AA}$  (Raman) and

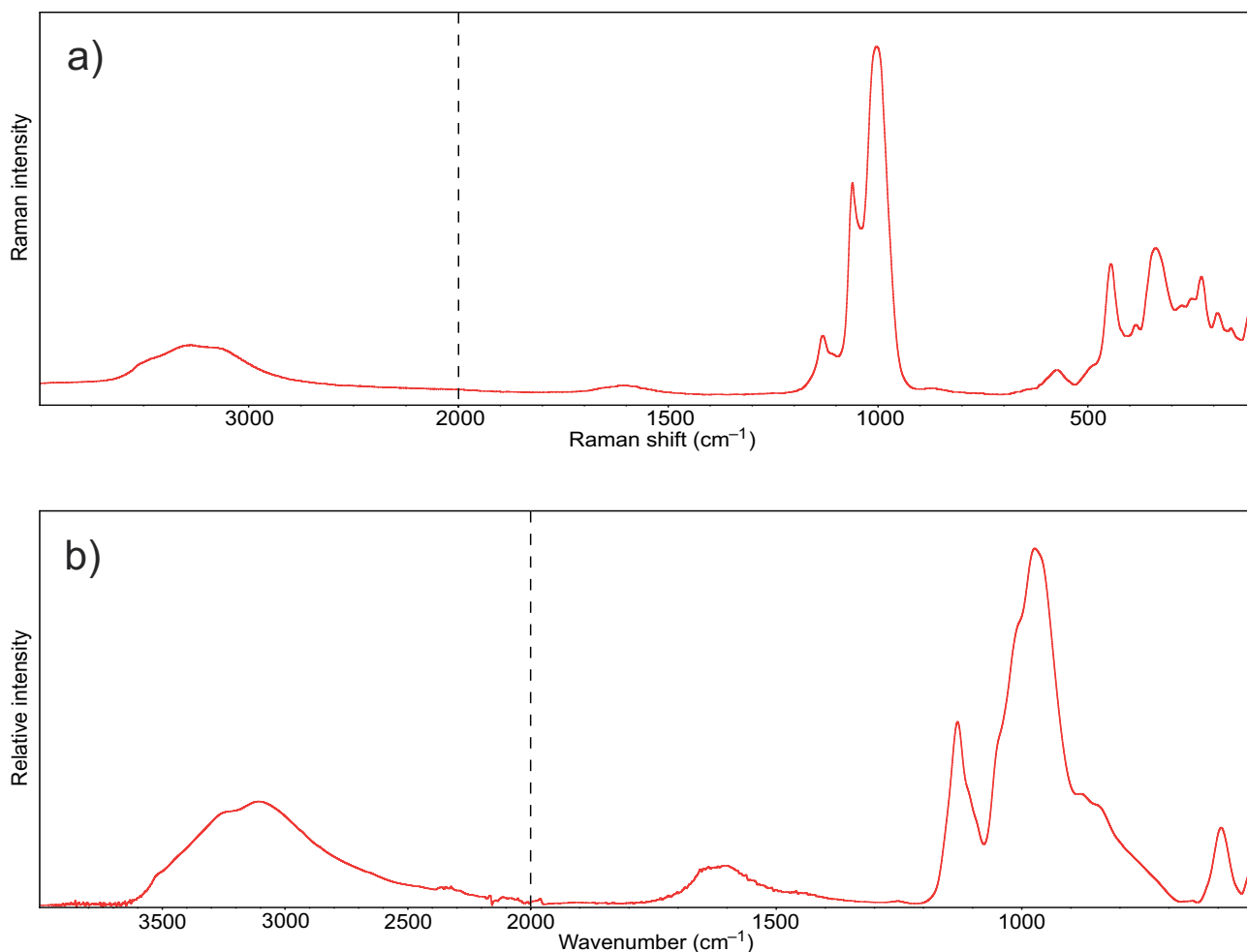


**Fig. 3a** – Raman spectrum of koninckite over the 50 to 4000  $\text{cm}^{-1}$  spectral range; **b** – infrared spectrum of koninckite over the 525 to 4000  $\text{cm}^{-1}$  spectral range; both spectra are split at 2000  $\text{cm}^{-1}$ .

3.2–2.6 Å (infrared). These values are practically comparable to hydrogen bond lengths, inferred from the single-crystal structure data of koninckite (Plášil et al. 2015).

A Raman very weak band at 1602  $\text{cm}^{-1}$  with some shoulders from 1679 to 1617  $\text{cm}^{-1}$  (Fig. 4b) and infrared bands at 1650 and 1598  $\text{cm}^{-1}$  (Fig. 5b) are attributed to the  $\nu_2$  ( $\delta$ ) bending vibrations of structurally distinct and differently strong hydrogen bonded water molecules. Raman shoulders from 1576 to 1520  $\text{cm}^{-1}$  and infrared shoulders at 1541 and 1454  $\text{cm}^{-1}$  could probably be connected with zeolitic-type free non-hydrogen bonded water located in channels of koninckite (Plášil et al. 2015). However, as usually known, any resolution of observed Raman weak and very weak bands and shoulders make problems. Some of them should be therefore probably understood as artefacts of the profile fitting procedure.

Raman medium bands at 1063, 1048 and 1015  $\text{cm}^{-1}$ , weak and very weak bands and shoulders at 1148, 1132 and 1108  $\text{cm}^{-1}$  (Fig. 4c) and an infrared medium band at 1131  $\text{cm}^{-1}$  with shoulders at 1097, 1049 and 1017  $\text{cm}^{-1}$  (Fig. 5c) are assigned to the  $\nu_3$   $\text{PO}_4^{3-}$  triply degenerate

antisymmetric stretching vibrations. The number of observed bands and shoulders proves  $T_d$  symmetry lowering connected with the splitting of the  $\nu_3$   $\text{PO}_4^{3-}$  triply degenerate vibrations and with two symmetrically distinct  $\text{P}^{5+}$  in the structure of koninckite (Plášil et al. 2015).

A Raman very strong band at 994  $\text{cm}^{-1}$  with a shoulder at 970  $\text{cm}^{-1}$  and an infrared medium strong band at 978  $\text{cm}^{-1}$  with a shoulder at 949  $\text{cm}^{-1}$  are attributed to the  $\nu_1$   $\text{PO}_4^{3-}$  symmetric stretching vibrations (Figs 4c, 5c). The number of the bands and shoulders relates to two  $\text{P}^{5+}$  present in the structure of koninckite (Plášil et al. 2015).

Infrared shoulders at 873, 833 and 748  $\text{cm}^{-1}$  (Fig. 5c) may be assigned to libration modes of water molecules (Frost et al. 2002).

A Raman medium band at 572  $\text{cm}^{-1}$  and very weak bands and shoulders at 670, 648, 631, 614 and 546  $\text{cm}^{-1}$  (Fig. 4d) and infrared weak and very weak bands at 592 and 534  $\text{cm}^{-1}$  (Fig. 5c), respectively, are connected with the split  $\nu_4$  ( $\delta$ )  $\text{PO}_4^{3-}$  triply degenerate out-of-plane bending vibrations and the  $\delta$  Fe–O bending vibrations. Chukanov (2014) observed corresponding bands at 606

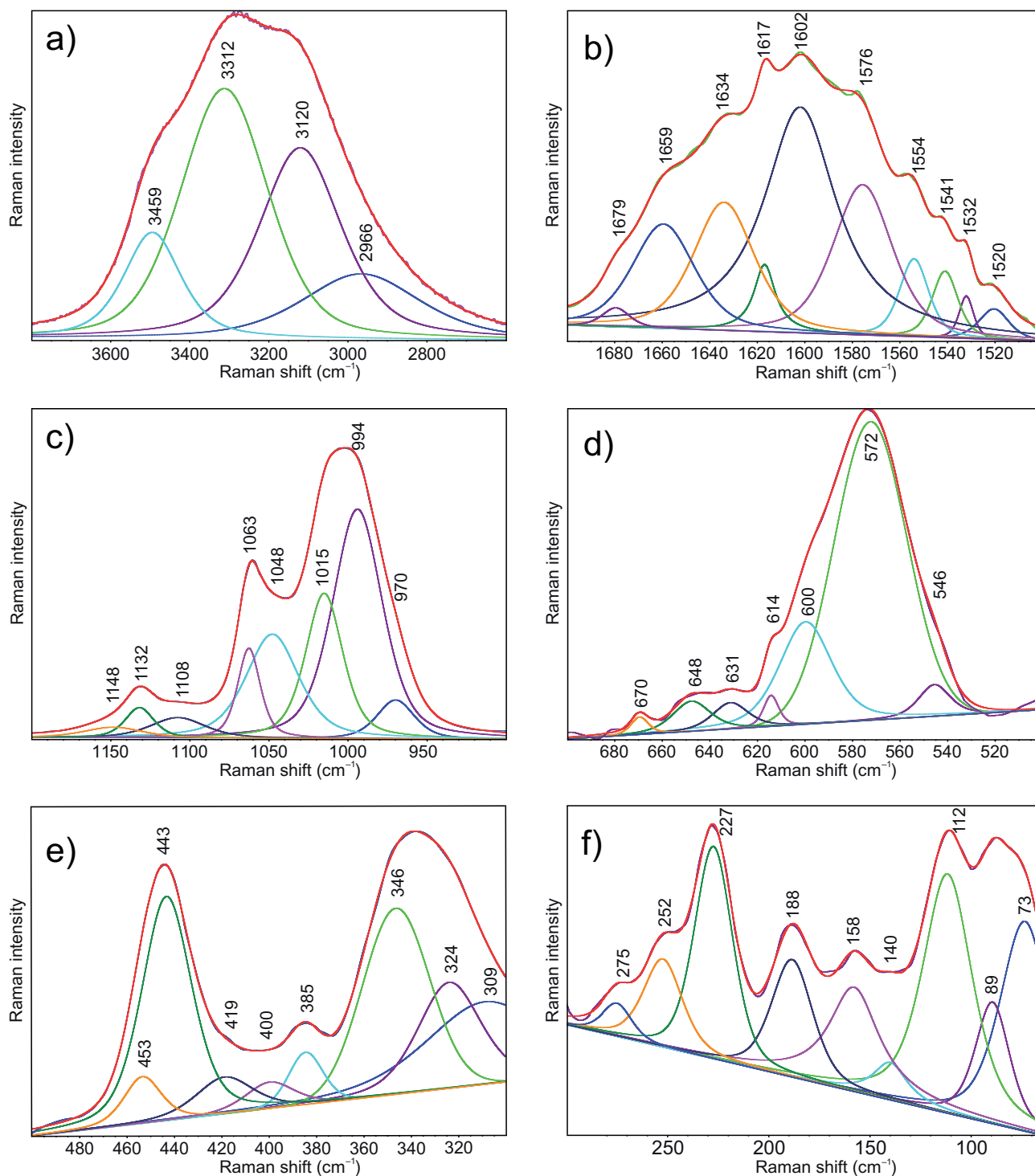
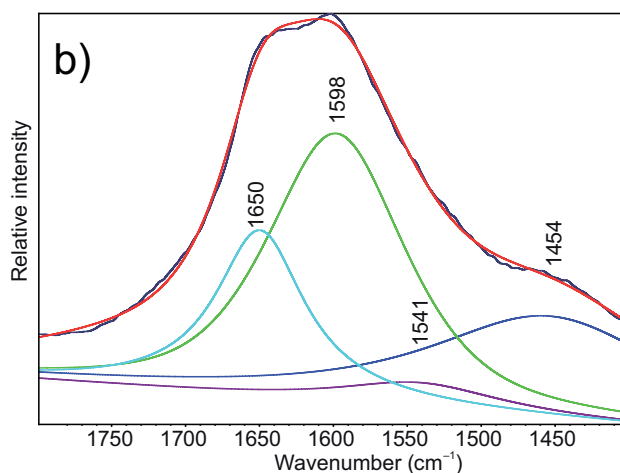
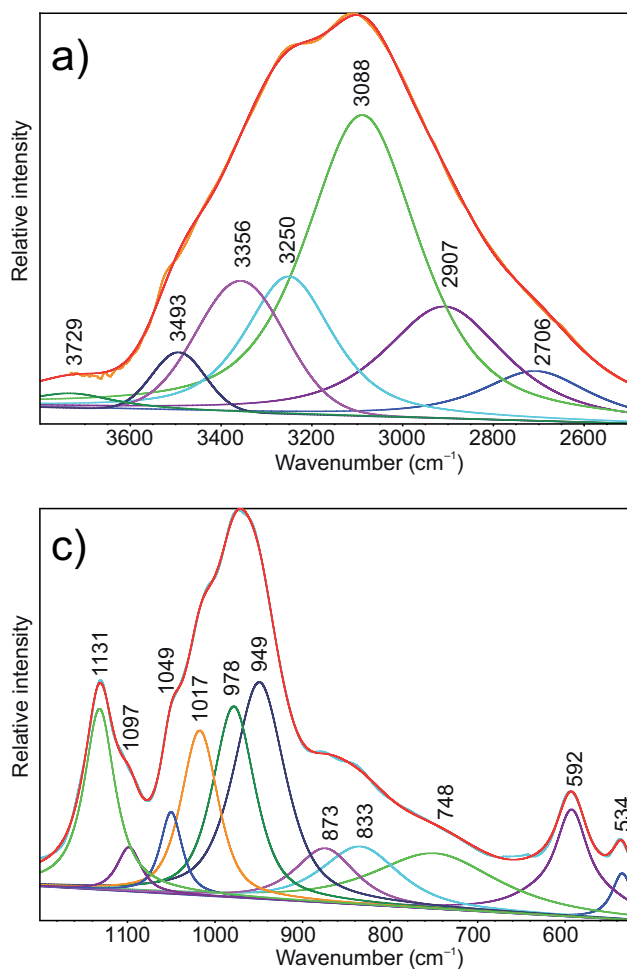


Fig. 4 Results of the band component analysis in the Raman spectrum of koninckite.

and  $540\text{ cm}^{-1}$  in the infrared spectrum of koninckite from Kociha, near Rimavská Sobota, Banská Bystrica District, Slovakia.

A Raman medium band at  $443\text{ cm}^{-1}$  with shoulders at  $453$ ,  $419$  and  $400\text{ cm}^{-1}$  are assigned to the split  $\nu_2(\delta)\text{ PO}_4^{3-}$  doubly degenerate bending vibrations (Fig. 4e). A Raman

medium bands at  $346$ ,  $324$ ,  $252$  and  $227\text{ cm}^{-1}$  and Raman weak bands at  $385$ ,  $309$  and  $275\text{ cm}^{-1}$  may be connected with  $\nu\text{ Fe-O}$  stretching vibrations in  $\text{FeO}_6$  octahedra. Raman medium and weak bands at  $188$ ,  $158$ ,  $140$ ,  $112$ ,  $89$  and  $73\text{ cm}^{-1}$  (Fig. 4e–f) are assigned to lattice vibrations (Čejka et al. 2011; Kerolli-Mustafa et al. 2013).



**Fig. 5** Results of the band component analysis in the infrared spectrum of koninckite.

supported by the Ministry of Culture of the Czech Republic (DKRVO 2017/02; National Museum 00023272) to JČ. The authors are grateful to Martin Števkó and an anonymous reviewer as well as the handling editor (Jiří Sejkora) for their constructive comments and suggestions, which substantially improved the quality of the manuscript.

#### 4. Conclusions

Molecular structure of koninckite can be better constrained using the vibrational spectroscopy. Raman spectroscopy shows the presence of  $\text{PO}_4^{3-}$ -units as identified by the position of the Raman peaks. The observation of multiple phosphate bands supports the concept of non-equivalent phosphate units in the koninckite structure. The presence of water is identified in the structure of koninckite by both Raman and infrared bands. Multiple water bands are observed showing that also water is involved in different coordination environments in the structure of koninckite due to differing hydrogen bond strengths.

*Acknowledgements.* Some of the analytical work was performed using equipment that was financed by the project “Institute of Clean Technologies for Mining and Utilisation of Raw Materials for Energy” (LO1406) and supported by the “Research and Development for Innovations Operational Programme” that is financed by structural funds of the European Union and the state budget of the Czech Republic. The study was financially

#### References

- BEUS AA (1950) Magnesiophyllite and manganokoninckite – new minerals from pegmatites from the Turkestan Range. *Dokl Akad Nauk SSSR* 73: 1267–1269 (in Russian)
- BEUS AA (1951) New phosphates from pegmatites from the Turkestan Range. *Trudy Mineral Muz Akad Nauk SSSR* 3: 19–36 (in Russian)
- BLASS G, GRAF H-W (1990) Neufunde von bekannten Fundorten. *Emser Hefte* 3: 82–85
- BLASS G, GRAF H-W (1995) Mineralogische Neuigkeiten vom Hardtkopf bei Sundern-Linnepe, Sauerland. *Mineralien-Welt* 4: 26–27
- CESÀRO G (1884) Sur la koninckite, nouveau phosphate ferrique hydrate. *Ann Soc Géol Belg* 11: 157–247
- CHUKANOV NV (2014) *Infrared Spectra of Mineral Species, Extended Library, Vol. 1*. Springer, Dordrecht, pp 1–1726
- ČEJKA J, SEJKORA J, PLÁŠIL J, BAHFENNE S, PALMER S, RINTOUL L, FROST RL (2011) A vibrational spectroscopic study of hydrated  $\text{Fe}^{3+}$  hydroxyl sulfates: polymorphic minerals butlerite and parabutlerite. *Spectrochim Acta A* 79: 1356–1363
- FROST RL, MARTENS W, WILLIAMS PA, KLOPROGGE JT (2002) Raman and infrared spectroscopic study of the vivianite-group phosphates vivianite, baricite and bobierite. *Mineral Mag* 66: 1063–1073

- FROST RL, LOPEZ A, XI Y, GRANJA A, SCHOLZ R (2013a) Vibrational spectroscopic characterization of the phosphate mineral kulanite  $\text{Ba}(\text{Fe}^{2+}, \text{Mn}^{2+}, \text{Mg})_2(\text{Al}, \text{Fe}^{3+})_2(\text{PO}_4)_3(\text{OH})_3$ . *Spectrochim Acta A* 115: 22–25
- FROST RL, PALMER SJ, XI Y, ČEJKA J, SEJKORA J, PLÁŠIL J (2013b) Raman spectroscopic study of the hydroxy-phosphate mineral plumbogummite  $\text{PbAl}_3(\text{PO}_4)_2(\text{OH}, \text{H}_2\text{O})_6$ . *Spectrochim Acta A* 103: 431–434
- FROST RL, SCHOLZ R, LOPEZ A, XI Y, DE SIQUEIRA QUEIROZ C, BELOTTI FM, FILHO MC (2014) Raman, infrared and near-infrared spectroscopic characterization of the herderite–hydroxyherderite mineral series. *Spectrochim Acta A* 118: 430–437
- IVANYUK GY, YAKOVENCHUK VN (1987) Minerals of the Kovdor Massif. Russian Academy of Science Kola Science Center Publishing, Kovdor-Apatity, pp 1–117
- JIRÁSEK J (2005) Find of koninckite near Litošice (Železné hory Mts.) in comparison with its world occurrences. *Bull Mineral-Petrolog Odd Nár Muz (Praha)* 13: 132–137 (in Czech)
- KEROLLI-MUSTAFA M, BAČIĆ I, ČURKOVIĆ L (2013) Investigation of jarosite process tailing waste by means of Raman and infrared spectroscopy. *Materialwiss Werkst* 44: 768–773
- KOCH S (1985) Minerals of Hungary. Akadémiai Kaidó, Budapest, pp 1–562 (in Hungarian)
- LEONARDOS OH, FERNANDES SM, FYFE WS, POWELL M (1987) The micro-chemistry of uraniferous laterites from Brazil: a natural example of inorganic chromatography. *Chem Geol* 60: 111–119
- LEUTE MA (1996) Mineralogische Neuigkeiten aus Österreich (1). *Mineralien-Welt* 3: 18–24
- LEUTE MA (1999) Mineralogische Neuigkeiten aus Österreich (3). *Mineralien-Welt* 5: 26–36
- LIBOWITZKY E (1999) Correlation of O–H stretching frequencies and O–H...O hydrogen bond lengths in minerals. *Monatsh Chem* 130: 1047–1059
- MERLET C (1994) An accurate computer correction program for quantitative electron probe microanalysis. *Microchim Acta* 114/115: 363–376
- MORETON S, GREEN DI (2005) Phosphate minerals including koninckite and planerite from Grouse Lodge Quarry, Shanagolden, Co. Limerick. *J Russell Soc* 8: 78–80
- NAKAMOTO K (2009) Infrared and Raman Spectra of Inorganic and Coordination Compounds, Part A: Theory and Applications in Inorganic Chemistry, 6<sup>th</sup> edition. Wiley, Hoboken, New Jersey, pp 1–432
- NOVÁK F, PAULIŠ P, ŠEVČŮ J, KOPISTA J, ZEMAN Z (2003) Koninckite, evansite, vashegyite and volborthite from Kociha near Rimavská Sobota (Slovakia). *Bull Mineral-Petrolog Odd Nár Muz (Praha)* 11: 159–166 (in Czech)
- PLÁŠIL J, MAJZLAN J, WIERZBICKA-WIECZOREK M, KIEFER B (2015) Crystal structure, thermal behaviour and paragenesis of koninckite,  $\text{FePO}_4 \cdot 2.75 \text{H}_2\text{O}$ . *Mineral Mag* 79: 1159–1173
- RIBA JR (1997) Montcada Hill (Montcada and Reixac, Vallès Occidental), history, mining and mineralogy. *Rev Mineral Catalun* 7: 34–55 (in Catalan)
- SAKURAI K, MATSUBARA S, KATO A (1987) Koninckite from the Suwa Mine, Chino City, Nagano Prefecture, Japan. *Bull Natl Sci Mus, Ser C* 13: 149–156
- SENEŠI F (2000) Koninckite and other phosphates from the Pollone Mine (Valdicastello Carducci, Lucca). *Riv Mineral Ital* 1: 46–48 (in Italian)
- SYMONS HH (1937) Minerals and statistics. *Calif J Mines Geol* 33: 251–253
- SZAKÁLL S (ed) (2002) Minerals of the Carpathians. Granit, Prague, pp 1–479
- SZAKÁLL S, GATTER I (1993) Mineral Species of Hungary. Fair System Kft., Miskolc, pp 1–211 (in Hungarian)
- VAN TASSEL R (1968) Données cristallographiques sur la Koninckite. *Bull Soc Fr Mineral Cr* 91: 487–489
- VON PUTTNER M (1997) Das seltene Phosphatmineral Koninckit in einer Mineralisation vom Geo-Trail bei Oberbuchach, Karnische Alpen (Kärnten). *Der Aufschluss* 48: 317–320

